PERGAMON

International Journal of Heat and Mass Transfer 43 (2000) 4249–4258

International Journal of HEAT and MASS TRANSFER

www.elsevier.com/locate/ijhmt

Nucleation site interaction during boiling

L.H. Chai, X.F. Peng*, B.X. Wang

Thermal Engineering Department, Tsinghua University, Beijing 100084, People's Republic of China

Received 14 June 1999; received in revised form 8 February 2000

Abstract

Classical analyses of boiling nucleation employ a linear approach with investigation focusing on a single site and the heat transfer obtained from the active site density assuming uniform wall superheat. This paper uses synergetic concepts and the self-organizing effect to analyze the interactions among active sites or bubbles induced by non-uniform temperature distribution, which depend mainly on boiling wall properties and thickness. Boiling experiments on the surface of different material plate walls with different thicknesses were conducted to reveal the nucleation site interaction. The results illustrate the experimental observations available in the literature and may provide a more reasonable mechanistic description of nucleation in boiling systems.

1. Introduction

Boiling is often encountered in a wide variety of applications, including traditional industrial processes, such as, metallurgical quenching, flooded tube-and shell evaporators, and immersion cooling of industrial components and modern heat transfer technologies used in space, electronic components, nuclear reactors, etc. The nature of boiling processes varies considerably depending on boiling conditions. The thermal boundary conditions, thermophysical properties of the medium, the wall material, and the size of the heated wall may all affect the boiling process. The importance of boiling in a wide variety of applications has provided an incentive for numerous investigations over the past decades. A substantial number of such efforts have been devoted to understanding and modeling the boiling heat transfer. A plethora of empirical correlations are available in the literature. However, a complete theory still eludes an effort, because the boiling phenomena are too complicated and have not been sufficiently understood.

In classical theories, the nucleate boiling heat transfer predictions still remain principally an empirical art and traditional modeling efforts typically use a linearized approach. For example, the physical phenomena are analyzed on the basis of a single site or vapor bubble, and the heat transfer rate is obtained for a given active site density distribution by assuming uniform conditions. The analyses assumed that the bubbles have no effect on the formation of adjacent bubbles. However, for practical boiling processes, interactions do occur between adjacent bubbles, and therefore, classical theory cannot be effectively related to macroscopic phenomena because it is based on individual discrete active sites.

The traditional linear approach conflicts with observations of phenomena such as, hysteresis, intermittent activity, deactivation of sites with increasing heat flux and interactions among sites [1]. This paper analyzes the interactions among active sites or bubbles using

* Corresponding author. Tel.: +86-10-6278-9751; fax: +86-10-6277-0209.

E-mail address: pxf-dte@tsinghua.edu.cn (X.F. Peng).

0017-9310/00/$ - see front matter
PII: S0017-9310(00)00055-7

Nomenclature

A	surface area
c	damping coefficient in Eq. (18a)
c_s	solid specific heat
G	Gibbs function
h_{fg}	latent heat
I	electric current
L	matrix defined in Eq. (23)
Q	amount of heat transfer
p	pressure
r	bubble radius
r_1	heat sink radius
t	time
T	temperature
u, v	vectors defined in Eqs. (21) and (28), respectively
U	voltage
z	axial coordinates

Greek symbols

ρ	density
σ	surface tension
λ	variable or thermal conductivity
α	thermal diffusion
φ	angular coordinate
θ	temperature excess
δ	thickness of plate
μ, μ'	integer 1,2,...,n

Subscripts

ave	average
c	critical
e	equilibrium
fg	liquid–vapor phase change
i	initial
l	liquid
s	saturated state
sup	superheat
v	vapor
w	wall

synergetics. Self-organization phenomena are also investigated. In addition, this paper presents the experimental results to reveal the underlying interaction mechanism.

2. Temperature variation induced by growing bubble

The active sites or bubbles, stochastically distributed on an arbitrary surface area, are schematically shown in Fig. 1. Physically, when a site becomes active and produces a bubble, the temperature in the surface around the active site will be influenced by the large amount of heat transferred to the growing bubble from heating surface due to evaporation of micro-layer underneath the bubble. Consequently, the behavior of adjacent sites will be affected. Therefore, nucleation at adjacent sites is interrelated and should not be modeled as independent, as is done in the literature [1]. Analysis of the interrelations between active sites is of both, practical and academic interest, but is still largely lacking in the literature. For a stochastic distribution of active sites or bubbles, as shown in Fig.1, the specific boundary conditions make it difficult to obtain exact theoretical solutions. The heat source method can be used to describe the heat transfer due to a single bubble. The phenomenon responsible for the interaction among active sites or bubbles could be modeled as a continuous surface heat sink drawing heat from the heating surface through evaporation of the micro-layer underlying the bubble.

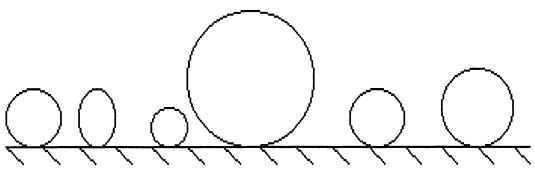

Fig. 1. Physical model.

For nucleate boiling, the formation of each embryo bubble may be idealized as a round continuous surface heat sink. Assuming the heating plate to be infinite with an initial temperature T_i, a point heat sink $P(r', \varphi', z')$ instantaneously absorbs heat Q, which will result in 3D unsteady heat conduction in the plate. With $\theta(r, \varphi, z, t) = T_i - T(r, \varphi, z, t)$, the temperature distribution in the cylinder coordinate system, can be represented as [2]:

$$\theta = \frac{Q/\rho c_s}{8(\pi\alpha t)^{3/2}} \exp\left(- \frac{r^2 + r'^2 - 2rr'\cos(\varphi - \varphi') + z^2}{4\alpha t} \right) \tag{1}$$

with a bubble radius contacting the surface of r_1 and a corresponding heat sink radius of r_1. A point heat sink $r'\,d\varphi'\,dr'$ at point (r', φ') instantaneously absorbs $Q_1 r'\,d\varphi'\,dr'/(\pi r_1^2)$ at time $t = 0$, where Q_1 is the total heat transfer for the embryo bubble per unit time [3].

The corresponding temperature decrease in the plate will be

$$d\theta = \frac{Q_1/(\pi r_1^2 \rho c_s)}{8(\pi\alpha t)^{3/2}} \exp\left(- \frac{r^2 + r'^2 - 2rr'\cos(\varphi - \varphi') + z^2}{4\alpha t}\right) r'\, d\varphi'\, dr' \quad (2)$$

The temperature decrease induced by a bubble generated on the surface should be equivalent to that induced by a heat sink with radius r_1. Therefore, the temperature decrease can be obtained by integrating

$$\theta(r, z, t) = \frac{Q_1/(\pi r_1^2 \rho c)}{8(\pi\alpha t)^{3/2}} \int_{r'=0}^{r_1}\int_{\rho'=0}^{2\pi} \exp\left(- \frac{r^2 + r'^2 - 2rr'cos(\varphi - \varphi') + z^2}{4\alpha t}\right) r'\, d\varphi'\, dr' \quad (3)$$

Using a particular case of Weber's second exponential integral [3],

$$\frac{1}{4\pi\alpha t}\int_{\varphi'=0}^{2\pi} \exp\left[- \frac{r^2 + r'^2 - 2rr'\cos(\varphi - ')}{4\alpha t}\right] d\varphi' = \int_0^\infty \exp(-\alpha\lambda^2 t) J_0(\lambda r) J_1(\lambda r_1)\, d\lambda \quad (3a)$$

Eq. (3) can be simplified to

$$\theta(r, z, t) = \frac{Q_1}{2\pi r_1 \rho c(\pi\alpha t)^{1/2}} \exp\left(- \frac{z^2}{4\alpha t}\right) \int_0^\infty \exp(-\alpha\lambda^2 t) J_0(\lambda r) J_1(\lambda r_1)\, d\lambda \quad (4)$$

where J_0 and J_1 are the Bessel functions of the first kind, order zero and one, respectively. Since the formation of each embryo bubble could be a continuous process, the temperature distribution resulting from a round continuous surface heat sink can be derived by integrating Eq. (4) with time, t, i.e.

$$\theta(r, z, t) = \frac{Q_1}{2\pi r_1 \rho c(\pi\alpha)^{1/2}} \int_0^\infty J_0(\lambda r) J_1(\lambda r_1) \left\{ \int_0 \exp\left[- \frac{z^2}{4\alpha(t - t')} - \alpha\lambda^2 (t - t')\right] \frac{dt'}{(t - t')^{1/2}} \right\} d\lambda \quad (5)$$

The final form is thus obtained as

$$\theta(r, z, t) = \frac{Q_1}{4\pi r_1 \kappa} \int_0^\infty J_0(\lambda r) J_1(\lambda r_1) \left[\exp(-\lambda z)\mathrm{erfc}\left(\frac{z}{2\sqrt{\alpha t}} - \lambda\sqrt{\alpha t}\right) - \exp(\lambda z) erfc\left(\frac{z}{2\sqrt{\alpha t}} + \lambda\sqrt{\alpha t}\right)\right] \frac{d\lambda}{\lambda} \quad (6)$$

Eq. (6) can be integrated numerically. The surface temperature distributions at $z = 0$ for copper and stainless steel plates are shown in Figs. 2 and 3. As seen in the figures, the initial temperature was taken as 110°C. Nucleation occurs as a site becomes active and the bubble grows, and the temperature field on the surface around the active site rapidly decreases with time, t, for much energy is transferred to the growing bubble from the surface by evaporation of the micro-layer underneath the bubble. Consequently, the nucleation at adjacent sites will also depress activation of the site and growth of the embryo bubble. Cooperative and competitive mechanisms exist between sites, with the results that the stronger and more preferred sites will be activated, while sites that are relatively weak and not activated will be depressed.

The bubble size and material properties significantly influence the temperature field. For larger bubbles (heat sink) on a stainless steel plate, the temperature decrease with time is faster and larger than for smaller bubbles on a copper plate, and the temperature field is more non-uniform. Therefore, smaller bubbles on plates having larger thermal conductivity will have less influence on nearby sites. It may be expected that the heating plate thickness and material properties will affect the interaction between bubbles and active sites.

3. Thermodynamic aspects of nucleation site interaction

Nucleate sites and bubbles interact to change the local superheat, which determines the stability of adjacent nuclei. As the formation of an embryo bubble, the change in the Gibbs free energy, ΔG, will be [4]:

$$\Delta G = \frac{4}{3}\pi r^3 \rho_v (G_v - G_l) + 4\pi r^2 \sigma \quad (7)$$

where G_v and G_l are the Gibbs free energy for vapor and liquid, σ is the surface tension, ρ_v is the vapor density, and r is the bubble radius.

Assuming that the bubble is in equilibrium with the surrounding liquid, the pressure difference across the interface satisfies the Young–Laplace equation

$$p_v - p_l = \frac{2\sigma}{r} \quad (8)$$

The pressure increase in the bubble can be obtained from the Clausius–Clapeyron equation, i.e.

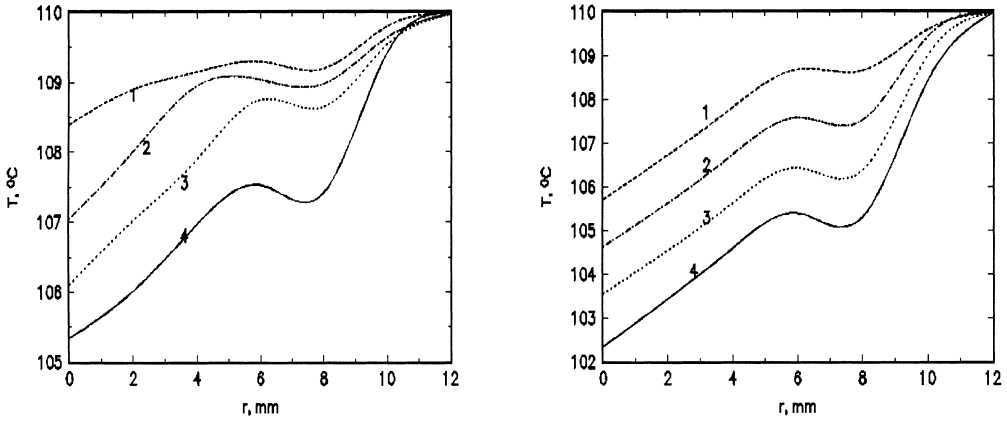

Fig. 2. Temperature distribution induced by growing bubble on copper plate (1: $t = 0.1$ s; 2: $t = 0.2$ s; 3: $t = 0.3$ s; 4: $t = 0.4$ s) (a) $r_1 = 1$ mm, (b) $r_1 = 2$ mm.

$$\frac{\Delta T_s}{\Delta p} = \frac{T_s}{h_{\mathrm{fg}}\rho_{\mathrm{v}}} \tag{9}$$

Substituting Eq. (8) into Eq. (9) yields

$$\Delta T_s = \frac{2\sigma T_s}{h_{\mathrm{fg}}\rho_{\mathrm{v}} r} \tag{10}$$

Hence, the bubble radius in equilibrium could be written as

$$r_{\mathrm{e}} = \frac{2\sigma T_s}{\Delta T_s h_{\mathrm{fg}}\rho_{\mathrm{v}}} \tag{11}$$

The derivative of Eq. (7) with respect to $r = 0$, yields

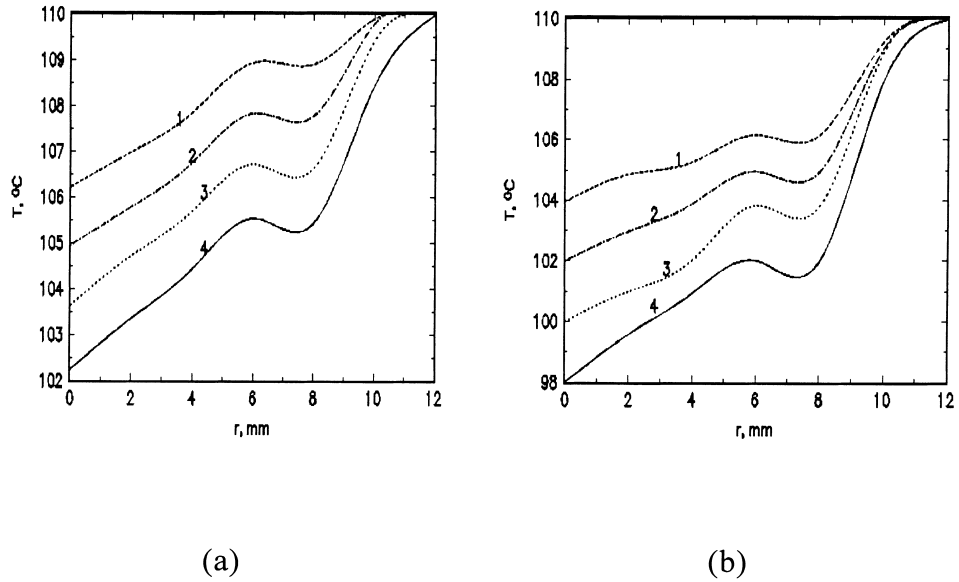

Fig. 3. Temperature distribution induced by growing bubble on stainless steel plate (1: $t = 0.1$ s; 2: $t = 0.2$ s; 3: $t = 0.3$ s; 4 = $t = 0.4$ s) (a) $r_1 = 1$ mm, (b) $r_1 = 2$ mm.

$$r_c = -\frac{2\sigma}{(G_v - G_l)\rho_v} \tag{12}$$

where r_c is the critical radius for a stable bubble. Since r_c in Eq. (11) and r_e in Eq. (12) are equal, we have

$$G_v - G_l = -\frac{h_{fg}\Delta T_s}{T_s} \tag{13}$$

Substituting Eq. (13) into Eq. (7), yields

$$\Delta G = -\frac{4\pi\rho_v h_{fg}\Delta T_s}{3T_s}r^3 + 4\pi\sigma r^2 \tag{14}$$

ρ_v, h_{fg}, ΔT_s, T_s, and σ are all constants for a given system. Since ΔG is a function of r only, there exists

$$\frac{dr}{dt} = -\frac{\partial \Delta G}{\partial r} = \frac{4\pi\rho_v h_{fg}\Delta T_s}{T_s}r^2 - 8\pi\sigma r \tag{15}$$

Eq. (15) defines the conditions for an embryo to grow if $dr/dt > 0$. This is the basis for analyzing synergetic phenomena in boiling systems. For convenience, Eq. (15) could be simplified to

$$\frac{dr}{dt} = -ar + br^2 \tag{16}$$

where $a = (8\pi\sigma)$ and $b = (4\pi\rho_v h_{fg}\Delta T_s/T_s)$. The first term on the right side of Eq. (16) is the fluctuation effect, while the second term is the evaporation effect. Due to interactions among multiple bubbles, both, the fluctuation term and evaporation term will be significantly changed.

As shown in Eq. (6), interactions among active sites or bubbles are reflected through only a site variable r — the nucleation radius. So, a set of equations of the form given in Eq. (16) that describe the growth rate of all bubbles are

$$\dot{r}_1 = -a_1 r_1 + b_1 f_1(r_1, r_2, \ldots, r_n)$$

$$\dot{r}_2 = -a_2 r_2 + b_2 f_2(r_1, r_2, \ldots, r_n)$$

$$\vdots$$

$$\vdots$$

$$\dot{r}_n = -a_n r_n + b_n f_n(r_1, r_2, \ldots, r_n) \tag{17}$$

where the second term on the right side is the evaporation effect, which is a function of multiple parameters when considering the interactions among numerous bubbles. Eq. (17) can be divided into two groups: $i = 1, 2, \ldots, m$, which are the weakly-damped modes with large b_i (meaning large ΔT_s) which may even be unstable ($b_i \to \infty$, for extremely large ΔT_s), and $s = m+1,\ m-2, \ldots, n$, which are the stable modes. Bubble growth is negligible for the stable modes, for $\dot{r} = 0$, and hence Eq. (17) can be written as

$$a_s r_s = b_s f_s(r_1, r_2, \ldots, r_m, r_{m+1}(r_i), \ldots, r_n) \tag{18}$$

which means $|r_s|$ that is induced by b_s is far less than $|r_i|$. Thus, for $s = m+1, m+2, \ldots n$, r_s in function f_s can be neglected.

In a real nucleating process in a boiling system, as described above, a single few modes in a specific unit will become unstable while most other modes will remain damped. The disturbance is induced by the superheat. We further propose that the superheat also affects the damped modes. Reducing the superheat increases the damping modes, such that the parameter with large superheats (weakly damped modes) dominantes the entire system behavior.

If the damping coefficients

$$c_i = a_i/b_i \tag{18a}$$

satisfy, $c_1 \gg c_2 \gg c_3 \gg \ldots$, the terms related to r_1 can be eliminated without affecting the other terms. The terms are then eliminated in succession, until only one variable remains.

4. Dynamic analysis of nucleation site interaction

For an arbitrary boiling system, in which the various parameters of Eq. (17) cannot be explicitly grouped, the embryo bubble growth rate can be rewritten as

$$\dot{r}_j = h_j(r_1, r_2, \ldots, r_n) \tag{19}$$

where h_j is a nonlinear function of r_1, r_2, $r_3, \ldots, r_n$. Interactions among active sites or bubbles are related to the unique variable — nucleation radius r. Taking the interactions among active sites or bubbles into account, for a steady-state solution of Eq. (19) given by r_j^0, the right side of Eq. (19) depends on a group of parameters β_1, β_2, $\beta_3, \ldots, \beta_n$, which are chosen in such a way that r_j^0 stands for stable values.

The origin of the r-coordinate system can be so shifted that

$$r_j^0 = 0 \tag{20}$$

For small perturbations, the unsteady results could be described as

$$r_j(t) = r_j^0 + u_j(t) \tag{21}$$

$$\vec{r}(t) = \vec{r}^{\,0} + \vec{u}(t) \tag{22}$$

where r is decomposed into a steady-state value and a perturbation. Eq. (19) will be linearized if the system is stable and u_j is sufficiently small, such that, by substituting Eq. (21) into Eq. (19), yields

$$\dot{u}_j = \sum_{j'} L_{jj'} u_{j'} \tag{23}$$

Matrix L_{jj} is a function of $\vec{r}^0$ and $\beta_1, \beta_2, \beta_3, \ldots, \beta_n$, or

$$\dot{\vec{u}} = L\vec{u} \tag{24}$$

Eq. (24) is the first-order ordinary differential equation with the solution

$$\vec{u} = \vec{u}^{(\mu)}(0)\exp(\lambda_\mu t) \tag{25}$$

Here, λ_μ are the eigen-values, i.e.

$$\lambda_\mu \vec{u}^{(\mu)}(0) = L\vec{u}^{(\mu)}(0) \tag{26}$$

$\vec{u}^{(\mu)}(0)$ is the right eigen-vector, and the generalized solution of Eq. (23) or (24) would be the superposition of Eq. (25), that is

$$\vec{u} = \sum_\mu \xi_\mu \exp(\lambda_\mu t)\vec{u}_\mu(0) \tag{27}$$

ξ_μ is an arbitrary constant. Introducing the left eigen-vector $\vec{v}^\mu L$ such that,

$$\lambda_\mu \vec{v}^{(\mu)} = \vec{v}^{(\mu)} L \tag{28}$$

If the system is stable, all the real parts of λ_μ will be negative, accordingly. If non-linear effects are to be considered, Eq. (24) will have the form

$$\dot{\vec{u}} = L\vec{u} + \vec{N}(\vec{u}) \tag{29}$$

where $\vec{N}(\vec{u})$ represents the nonlinear contribution. If u is still expressed in the form given by Eq. (27), then, the appropriate expression $\xi(t)$ must be found so that the following relation is satisfied with left multiplying Eq. (29)

$$\langle \vec{v}^{(\mu)}, \vec{u}^{(\mu')} \rangle = \delta_{\mu\mu'} \tag{30}$$

and Eq. (29) becomes

$$\xi_\mu = \lambda_\mu \xi_\mu + g_\mu(\xi_1, \xi_2, \ldots, \xi_n) \tag{31}$$

where $g_\mu = \langle \vec{v}^{(\mu)}, \vec{N}(\sum_\mu \xi_\mu \vec{u}^{(\mu)}) \rangle$

Eq. (31) has the same form as Eq. (17), so that one or a few λ_μ are equal to or greater than zero while the others have a negative real part and thus are relating to the damping modes. If mode ξ_r for $Re(\lambda_\mu) \geq 0$ is sufficiently greater than other modes, then, adiabatic elimination can be used to simplify the system.

The analysis is in good agreement with observed nucleation phenomena. Numerous active sites exist on surface, however, only a few can nucleate and produce visible bubbles while most embryo bubbles will rapidly disappear. When one mode does not dominate the others, flashing will occur. Flashing is likely to occur when $c_1 \approx c_2 \approx c_3 \approx \ldots c_n$.

The self-organized transition process from natural convection to nucleate boiling, which can be analyzed with this theory, is a transition from a state characterized by disordered liquid molecule motion to another state characterized by liquid–vapor molecule interaction. The system becomes more ordered with nucle-

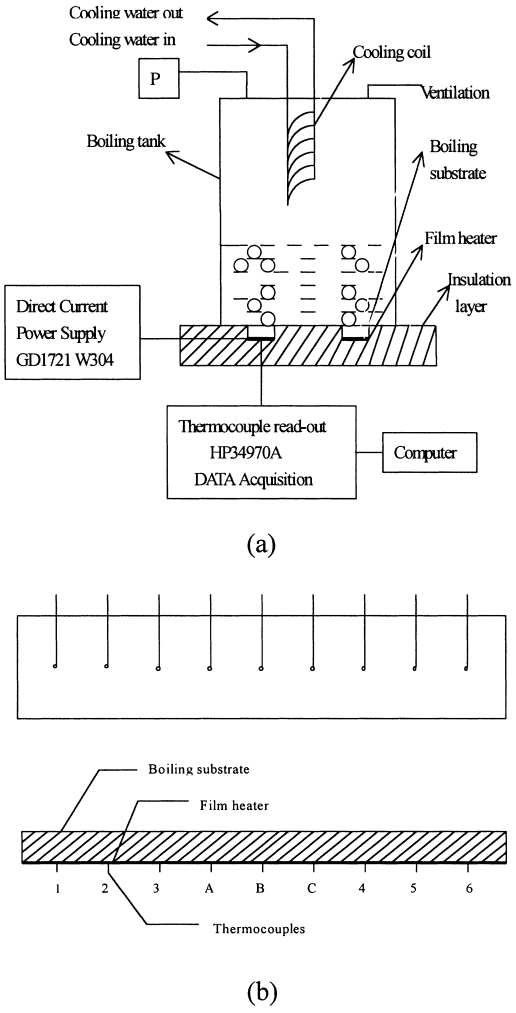

Fig. 4. Experimental apparatus (a) Schematic diagram of experimental setup, (b) boiling surface (20 mm × 60 mm, thermocouples are installed in equal distances).

ate boiling system as a typical dissipative structure. The analysis provides a vivid picture of the formation of this kind of ordered dissipative structure.

5. Experiments

The pool nucleate boiling experiments on the surfaces of different material metal plate with different thickness were conducted to investigate the nucleation site interaction.

5.1. Experimental apparatus

The schematic of the experimental set-up is shown in Fig. 4(a), which mainly consists of test section, liquid tank, power supply, measurement system, and cooling loop.

The liquid tank was made of a circular Pyrex vessel with height 120 mm and inside diameter 110 mm. The bottom plate of the tank was insulated into the channels of which two 20×60 mm rectangular metal plates were symmetrically placed as boiling substrates, and sealed with 704-silicone rubber. Eight copper–constantan (T-type) thermocouples were uniformly embedded into the bottom of the metal plates to measure the boiling surface temperature, as shown in Fig. 4(b). Film heaters of 9.00, 9.04, 9.04 and 8.95 ohms, respectively, were coated onto the bottom side of the metal plates.

Four kinds of test sections are used in the experiments. Two were made of aluminum plates having thicknesses 6 and 11 mm, and the other two were made of 0.13C–12.95Cr–0.14Ni stainless steel plates having thicknesses 6 and 11 mm. Liquid methanol, ethanol and *n*-pentane were used as the boiling fluids.

A GD1721 DC power supply was connected in series with a standard resistor and film heater. The resistor was used to measure the electric current, and provide the desired heat flux by adjusting the voltage input.

The data acquisition system includes one 16-channel input module (14 for thermocouple and two for voltage and electric current), whose uncertainty is estimated to be 0.1% as provided by the manufacturers, and a RS232 interface is connected to a personal computer.

A water-cooled coil was used to condense the vapor generated, so as to minimize the loss of test liquid and stabilize the system pressure. Atmospheric pressure was maintained by venting the test vessel to ambient. The U-type pipe was used to monitor the pressure in the vessel. The whole test section was well insulated for minimizing the heat loss.

5.2. Data reduction

The parameters required to measure in these experiments are the boiling wall temperature, the voltage drop U across the film heater and the system electric current I. The heat flux was calculated by the measured voltage drop, U, across the film heater and the system electric current, I, as

$$q'' = UI/A \tag{32}$$

Time–area averaged temperature is defined as

$$\bar{T} = \frac{1}{At}\int_A \int_t T \, \mathrm{d}A \, \mathrm{d}t. \tag{33}$$

The bottom time–area averaged temperature of the boiling substrates can be obtained by data acquisition system, and then, the boiling wall surface time–area averaged temperature can be correlated by 1D heat conduction model at each applied heat flux as

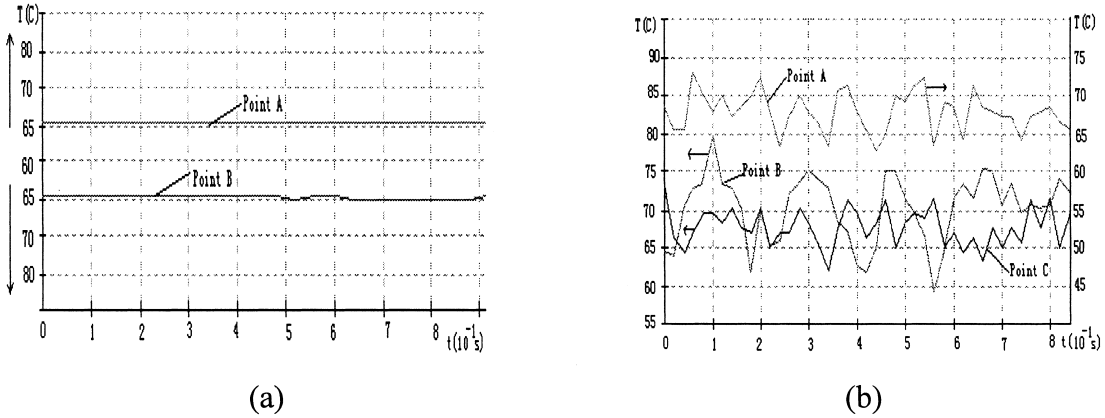

Fig. 5. Wall temperature history (a) for free convection, (b) for nucleate boiling (q = 16.75 kW/m^2).

$$\bar{T}_w = \bar{T} - q''\delta/\lambda \tag{34}$$

with wall superheat obtained as

$$\Delta\bar{T}_{sup} = \bar{T}_w - T_s \tag{39}$$

The experimental system was started up with no power input, and then made to run at a small power supply until the test liquid reaches its saturation temperature. Increasing the voltage input of DC power gradually gives the desired heat flux. The test section is considered to be at steady conditions if the temperature variations for all thermocouples were less than 0.2 K. The temperatures of all measured points was then recorded for the measured voltage and current.

The uncertainty of heat flux owing to heat losses from substrate was estimated to be less than 10%. The uncertainty in temperature was estimated at about 8%. Repeated experiments show that the reproduction was satisfactory.

5.3. Results and discussion

The temperature histories are obtained by data acquisition systems to investigate the temperature wavy characteristics and thermal interactions. Fig. 5 shows the situation before and after the occurrence of boiling for methanol liquid. Very clearly, the wall temperatures are quite stable for single-phase free convection.

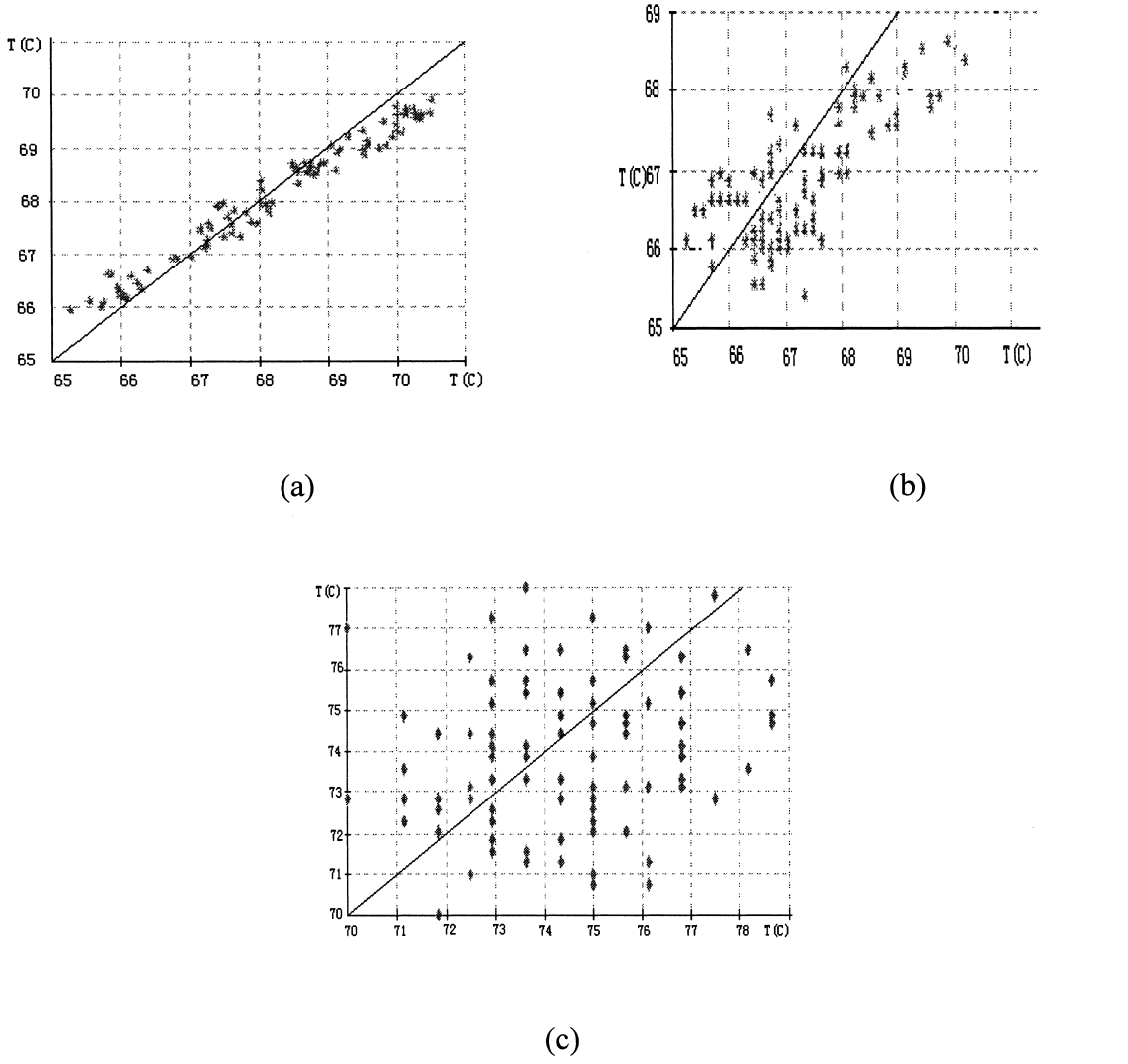

Fig. 6. The temperature relation at two adjacent points (Points B and C) (a) Aluminum, b = 11 mm, (b) Aluminum, b = 6 mm, (c) Stainless steel, b = 6 mm.

The unstable non-uniformity appears when the nucleate boiling occurs. The performance of the wall temperatures for different positions is very similar, but not in the same chronology. The wavy fluctuations of wall temperature with significant amplitude and irregular period/frequency can be attributed to the thermal interactions. Either the nucleation and/or the bubble departure at the same point or at adjacent sites may induce the temperature behavior at that specified location [5]. The wavy characteristics become more evident with the increasing applied heat flux. Therefore, the nonlinear thermal interactions will become more evident with the increased applied heat flux.

The thermal interactions will be definitely influenced by the wall properties and thicknesses as well. To explore the temperature interrelationship of two adjacent positions, the temperatures at two adjacent points are obtained by data acquisition system, represented by x-axis and y-axis, respectively. The typical results for methanol liquid boiling on different plates is shown in Fig. 6. Deviations from the diagonal indicate the degree of the thermal interaction. The thinner the plate and the smaller the plate thermal conductivity, the stronger the thermal interactions will be. From the comparison, thermal conductivity of the heating surface may play a more critical role for thermal interaction.

The thermal interactions influence the active site

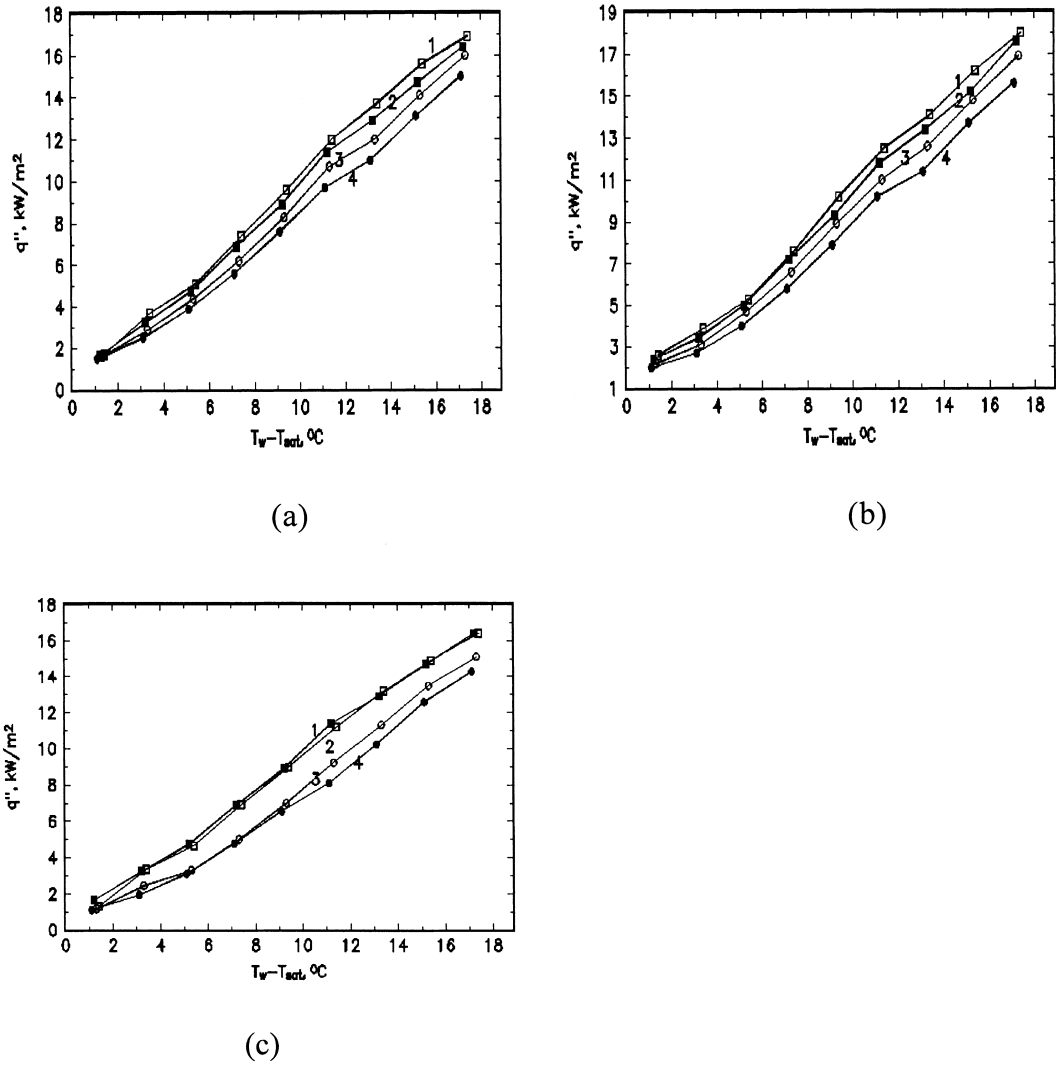

Fig. 7. Experimental data of pool nucleate boiling (1: 11 mm aluminum; 2: 6 mm aluminum; 3: 11 mm steel; 4 = t = 6 mm steel (a) for methanol, (b) for ethanol, (c) for n-pentane).

density and associated nucleate boiling heat transfer. The typical results of boiling experiments of liquid methanol, ethanol and *n*-pentane are illustrated in Fig. 7. At the same superheat, the heat flux for plate having higher thermal conductivity could be greater than that having lower thermal conductivity. Simultaneously, at the same superheat, the heat flux for thicker plate could be greater than the thinner one. In reality, the thermal interaction for better thermal conductivity and thicker plate will become weaker and have less influence in decreasing the heat transfer.

So far, the researches on pool nucleate boiling heat transfer are mostly focused on the wall surface characteristics, such as, micro-geometry, roughness and wettability. However, the scatter and deviation in experimental data is not just only caused by surface characteristics and measuring uncertainty. Apparently, both, surface characteristics (roughness, aging, wettability) and bulk characteristics (substrate properties, thickness) are also the aspects necessary to be included for nucleate boiling heat transfer. The bulk effects on boiling heat transfer will arise in two different ways: Firstly, the decrease in wall temperature due to the nucleation bubble growing affects the time period, and associated heat transfer. This is reflected in penetration distance, which is of the order 1.5 mm for aluminum and 0.4 mm for stainless steel, respectively. It can be expected that, the boiling heat transfer coefficient will be independent of plate thickness if the thickness exceeds the penetration distance. Secondly, the decrease in wall temperature due to the nucleation bubble growing activates adjacent nucleate site, and thus changes the bulk boiling heat transfer performance. This is the so-called thermal interaction. In the present experiments, thicknesses of 6 and 11mm, respectively, are much larger than the according penetration distance. Obviously, the differences in boiling heat transfer are mainly caused by the thermal interactions.

6. Conclusions

Classical analyses on nucleation employs a linear approach with nucleation phenomena analyzed on the basis of a single site, and the active sites density used to obtain macroscopic results with the assumption of uniform wall superheat. The basic concepts of synergetics have been used to analyze the interactions among active sites or bubbles, and the self-organizing processes during nucleation. Experiments for pool nucleate boiling on heated plate wall with several different material and thickness were conducted to reveal the nucleation site interaction. The present investigation shows more reasonable mechanistic descriptions of nucleation in boiling systems and provides a renewed effort to understand the fundamentals of boiling.

Acknowledgements

The project was supported by the National Natural Science Foundation of China through contracts #59625612, #59976016 and #59995550-3.

References

[1] M. Shoji, Boiling chaos and modeling, in: Proceeding of 11th International Heat Transfer Conference, vol. 1, Taylor and Francis, Korea, 1998, pp. 3–21 (Invited Keynotes).
[2] H.S. Carslaw, J.C. Jaeger, Conduction of Heat in Solids, 2nd ed., Clarendon Press, Oxford, 1986, pp. 255–263.
[3] P.H. Thomas, Some conduction problems in the heating of small areas on large solids, Quart., Journ. Mech. and Applied Math. 10(4), (1957).
[4] Van P. Carey, Liquid Vapor Phase-Transition Phenomena, Hemisphere, Washington, 1992.
[5] D.B.R. Kenning, Y.Y. Yan, Pool boiling heat transfer on a thin plate: features revealed by liquid crystal thermography, Int. J. Heat Mass Transfer 39 (15) (1996) 3117–3137.